AIAA Guidance, Navigation and Control Conference and Exhibit
18 - 21 August 2008, Honolulu, Hawaii

AIAA 2008-7253

Electro-Optical System Analysis for Sense and Avoid*

J. Daniel Griffith†, Mykel J. Kochenderfer‡,
and James K. Kuchar§

Lincoln Laboratory, Massachusetts Institute of Technology, Lexington, MA 02420

This paper presents a parametric analysis of the sense and avoid capability for an electro-optical system on unmanned aircraft. Our sensor analysis is based on simulated encounters from a new U.S. airspace encounter model that provides a comprehensive distribution of typical visual flight rule (VFR) aircraft behavior and encounter geometries. We assess the exchange between the sensor field-of-view shape and detection range with the probability of intruder detection prior to near miss. This assessment also includes a trade-off analysis between field-of-view azimuth angle and probability of detection with fixed tracking technology (i.e. pixel array sensor and tracking algorithm). Initial results suggest that current standards are suitable for detecting larger aircraft but may not be ideal for small aircraft such as ultralights.

I. Introduction

Northrop Grumman and the Air Force are considering a variety of sensors onboard Global Hawk for a collision avoidance system (CAS). These include the Traffic alert and Collision Avoidance System (TCAS), automatic dependent surveillance-broadcast (ADS-B), electro-optical (EO) and infrared (IR) systems, and radar. TCAS and ADS-B provide a satisfactory means of sensing transponder-equipped aircraft but lack the ability to detect aircraft that are not equipped with a transponder. EO, IR and radar sensors are appealing solutions for detecting traffic because they do not require that intruders have special equipage. EO and IR systems are particularly attractive for unmanned aircraft since their power requirements and payload sizes are smaller than radar systems.

The current Global Hawk EO concept utilizes a three camera system to detect intruder aircraft. In designing such a system there are two important design factors: the solid angle subtended by the field-of-view (FOV) and detection range. An ideal EO sensor provides a FOV that subtends 4π steradians with infinite detection range, but full coverage may require an infeasible number of cameras. Detection range is also limited by factors such as camera technology, intruder aircraft size, and atmospheric conditions. Trade-offs exist between these design parameters. In general, increasing the FOV reduces detection range and vice versa.

This document describes a trade analysis of EO sensors to provide a sense and avoid capability. The results presented in this paper are intended to facilitate current and future collision avoidance system design decisions for Global Hawk or other unmanned aircraft. In this study we evaluate the FOV and detection range trade-offs based on the probability of an intruder being detected for varying EO sensor configurations. The analysis in this document is derived from a new encounter model developed at Lincoln Laboratory based on radar data from across the United States.[1]

The following section discusses the current sense and avoid requirements for unmanned aircraft in U.S. airspace and the current EO design configuration for Global Hawk used in previous flight tests that provides a baseline for this study. Section III describes the encounter model that we use for our analysis. Section IV discusses trades between FOV and detection range with fraction of intruders detected. Finally, Section V analyzes the direct tradeoff between the FOV azimuth angle and fraction of intruders detected for a fixed

*This work is sponsored by the Air Force under Air Force Contract #FA8721-05-C-0002. Opinions, interpretations, conclusions, and recommendations are those of the authors and are not necessarily endorsed by the United States Government.

†Associate Staff, Surveillance Systems, 244 Wood Street.
‡Technical Staff, Surveillance Systems, 244 Wood Street.
§Assistant Group Leader, Surveillance Systems, 244 Wood Street. Senior Member AIAA.

sensor array and detection technology. Results from the sensor trade-off analysis suggest that the current EO sensor configuration is suitable for detecting larger aircraft (i.e. Boeing 737s and larger) with enough lead time for a CAS to identify the intruder aircraft and initiate a resolution action in simulation. However, the current sensor configuration may not be ideal for detecting smaller aircraft such as ultralights and Cessna 172s. In fact, reducing the FOV improves the likelihood of a smaller intruder being detected prior to near miss in this study.

II. Sense and Avoid Status

A white paper issued by Air Combat Command defines sense and avoid requirements for unmanned aircraft that require access to civil airspace without a Federal Aviation Administration (FAA) Certificate of Authorization (COA).[2] The purpose of the white paper is to provide an initial, formal sense and avoid requirement for unmanned aircraft to ensure that they comply with all applicable regulations for operating in all classes of airspace.[3] The white paper's sense and avoid requirements for FOV are based on both NASA and Department of Defense studies, as well as the Convention on International Civil Aviation, Annex 2, Rules of the Air, and stipulate $\pm 110^\circ$ in azimuth and $\pm 15^\circ$ in elevation.[4]

The current $\pm 15^\circ$ elevation angle requirement is based on safety analyses performed by NASA and the Department of Defense that showed this angle was suitable for head-on encounters where the intruder has a flight path angle up to 20° (higher than most typical flight paths). The $\pm 110^\circ$ azimuth angle requirement was chosen to meet current flight rules. According to the ICAO Rules of the Air, if an intruder is outside the $\pm 110^\circ$ azimuth angle, then this type of an encounter is considered an overtaking encounter rather than a converging encounter. Both aircraft have responsibility to follow the rules of the air and avoid a collision in a converging encounter. However, in the case of overtaking encounters, it is solely the responsibility of the overtaking aircraft to avoid a collision. Currently there is limited safety analysis to support that a $\pm 110^\circ$ azimuth angle is sufficient to provide an equivalent level of safety as having a pilot in the cockpit. Finally, the detection range requirement for sense and avoid is such that the CAS is able to process the sensor information, determine if a hazard exists, and perform a successful collision avoidance maneuver.

The white paper notes that the current requirements may change if future safety analyses, operational testing, or demonstrations reveal a different FOV can provide a higher level of safety. In addition, the white paper admits that it may be financially infeasible to meet the sense and avoid requirements for testing of a CAS.

The Air Force Research Laboratory (AFRL) and Defense Research Associates (DRA) are collaborating on an EO-based system for detecting intruder aircraft to demonstrate sense and avoid capabilities for Global Hawk. The current, flight-tested EO sensor on Global Hawk has three cameras that provide a FOV with dimensions $\pm 100^\circ$ by $\pm 15^\circ$. This FOV was chosen because off-the-shelf components could be used at a fraction of the price of designing a custom system with an azimuth angle of $\pm 110^\circ$. In addition, each camera is equipped with a 2048 by 1024 pixel silicon focal plane array.[5]

We use this Global Hawk EO sensor configuration as a baseline in this analysis. We assume that the cameras' coverage do not overlap and the image plane is uniform over the entire FOV. Both the azimuth angle and elevation angle are defined from the nose of the aircraft with no aircraft angle of attack and are fixed to the aircraft's body axis. In addition, each baseline camera is equipped with a 2000 by 1000 pixel detection array, which amounts to a combined 6000 by 1000 detection array over the entire FOV. Our analysis of the EO sensor configuration parameters is two-fold and is based on encounters that result in a near mid-air collision, which is a loss in separation of at least 100 ft vertically and 500 ft horizontally at the same time. First, we consider the fraction of NMAC-causing intruders being detected with various azimuth, elevation, and range values to evaluate the performance of the current configuration and determine where any design changes may be made to improve sensor performance. Next, we evaluate the effect that changing the FOV azimuth angle has on the fraction of intruders detected with fixed camera and detection technology. Note that this initial analysis is based on a binary value: either an intruder is in view or it is not at each timestep. The purpose of this study is to analyze trade-offs between azimuth angle, elevation angle, and detection range based on a statistical representation of encounters in the U.S. airspace; we do not consider computer vision performance or the detection software. In practice, detecting an intruder is much more complex due to atmospheric conditions, contrast or target signal strength, and false tracks. The detection software will often require a period of time to discriminate an intruder from false tracks. Other studies have investigated detection algorithm performance through flight tests and archived images from EO sensors.[6,7]

III. Encounter Generation

The analysis provided in this paper uses Lincoln Laboratory's Collision Avoidance System Safety AssessmenT Tool (CASSATT) to simulate encounters that are statistically representative of intruder aircraft behavior based on a preliminary non-cooperative encounter model under development at Lincoln Laboratory.[1] To build our model, we collected visual flight rules (VFR) beacon reports (Mode A code 1200) between December 1, 2007 and December 7, 2007. This amounts to 30,109,411 reports representing 78,000 flight hours from across the United States. The raw radar reports are first processed using a tracking algorithm developed at Lincoln Laboratory.[8] A fusion algorithm, also developed at Lincoln Laboratory,[9] then fuses tracks from multiple sensors to provide a single global view of all the tracks in U.S. airspace. We build a statistical model of aircraft behavior from the collected VFR tracks using a Bayesian network.

An encounter occurs when an intruder penetrates an encounter cylinder centered on the aircraft. The appropriate size for the encounter cylinder is determined by the aircraft dynamics and CAS. If the cylinder is too small, then the CAS does not have sufficient time to detect and track an intruder; however, if the cylinder is too large, then computation is wasted. Aircraft are initialized on the surface of the encounter cylinder based on the assumption that the distribution of aircraft outside of the cylinder is uniformly random.

We used two collections of 1 million encounters each as the basis for our analysis. One collection consists of encounters between pairs of VFR aircraft generated by the encounter model. Figure 1 shows histograms of the initial trajectory characteristics. The other collection consists of encounters between Global Hawk and VFR aircraft. The Global Hawk trajectories are a mixture of four profiles, as shown in table 1. The first two profiles were extracted from radar data of an actual Global Hawk flight. The other two profiles were based on Global Hawk performance specifications.

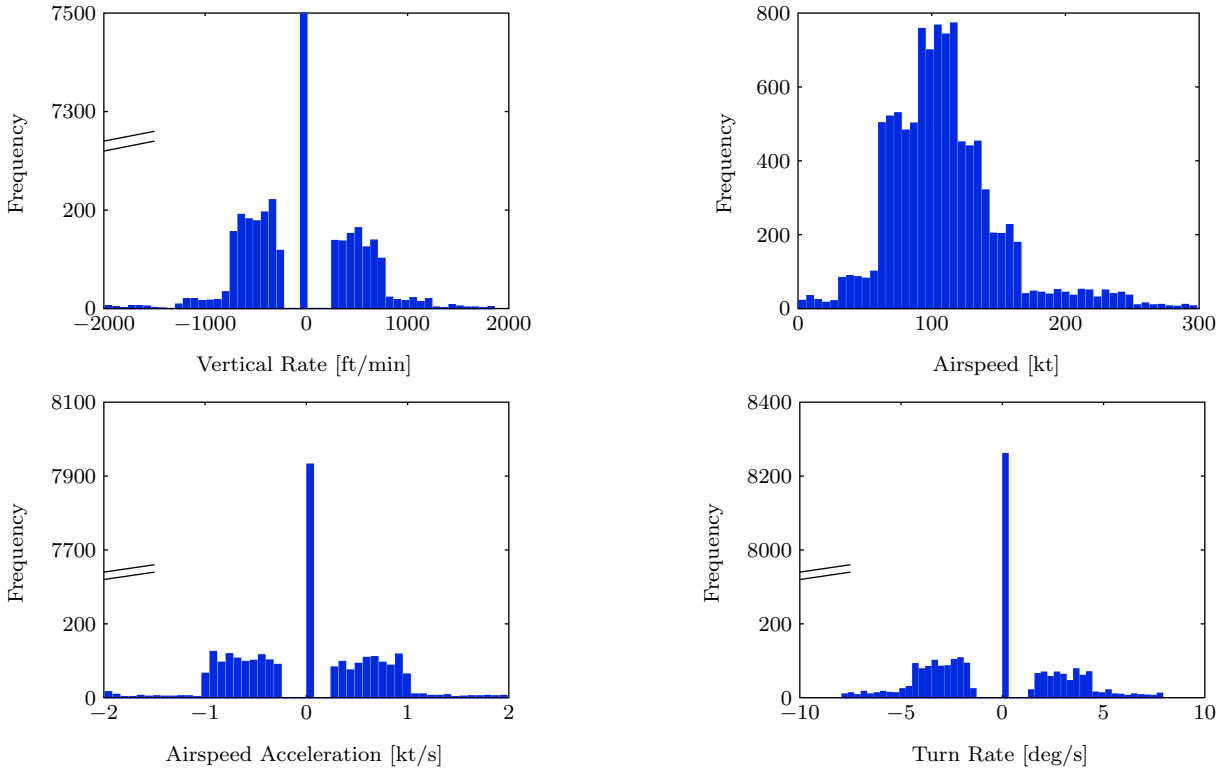

Figure 1. Histograms of VFR track characteristics.

We used a larger encounter cylinder height for encounters involving Global Hawk because the airspeed and vertical rates of Global Hawk are typically greater than most VFR aircraft. Table 2 summarizes the characteristics of the two encounter sets. Of particular note is that the minimum simulation time until time of minimum cylindrical distance (TMCD)[a] for the encounter sets is over 27 s, which is sufficient time for a CAS to sense and avoid an intruder. TMCD is used as a surrogate for time of minimum separation to correct for the fact that smaller vertical miss distances are acceptable relative to lateral distances. Figure 2

[a]Cylindrical distance is $\max(r_h/5, r_v)$, where r_h is horizontal range and r_v is vertical range.

Table 1. Profiles used to generate Global Hawk trajectories. The first two profiles in the table have average climb rate, turn rate, and airspeed listed since they vary during the course of the trajectory. All other values in the table are constant.

Mixture	Climb rate	Turn rate	Airspeed
25%	3392 ft/min	1.5 deg/s	191 kt
25%	-1279 ft/min	0.2 deg/s	145 kt
25%	3100 ft/min	0 deg/s	170 kt
25%	-1300 ft/min	0 deg/s	150 kt

presents the initial bearing histograms of the intruders initialized on the side of the encounter cylinder in each collection of encounters. The distribution of intruders is more concentrated towards zero bearing for Global Hawk than for VFR aircraft because the airspeed of Global Hawk is higher than that of most VFR aircraft in our model. Thus, intruders are less likely to overtake Global Hawk. Figure 2(c) demonstrates the relationship between own aircraft airspeed and distribution of intruders on the side of the encounter cylinder. When the own aircraft's airspeed is near zero, the intruders are approximately evenly distributed around the encounter cylinder. In contrast, if the own aircraft's speed is 220 kt, approximately 50% of the intruders are within a bearing angle of $\pm 50°$.

Table 2. Characteristics of the two collections of 1 million encounters used for our analysis.

	VFR/VFR	Global Hawk/VFR
Encounter cylinder radius	5 NM	5 NM
Encounter cylinder height	± 1500 ft	± 3300 ft
Minimum TMCD simulation time	27.9 s	30.4 s
Mean TMCD simulation time	166.4 s	89.4 s
NMACs	541	364

Each encounter simulation provides time histories of position, velocity, attitude, and body rates for each aircraft and is run open-loop without any CAS enabled. We model the intruder range in addition to elevation angle and azimuth angle in the own aircraft camera's FOV. We also calculate the projected visual area of intruder aircraft using a three-dimensional polygon model of the airframe.

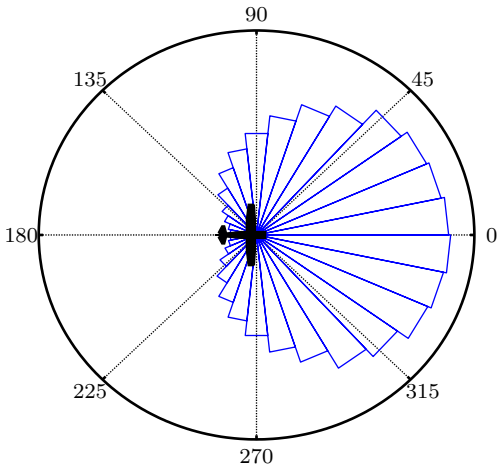

(a) Bearing distribution of 604,637 intruders initialized on the side of the encounter cylinder for VFR/VFR encounters. The remaining 395,363 intruders are uniformly distributed on the top and bottom of the cylinder.

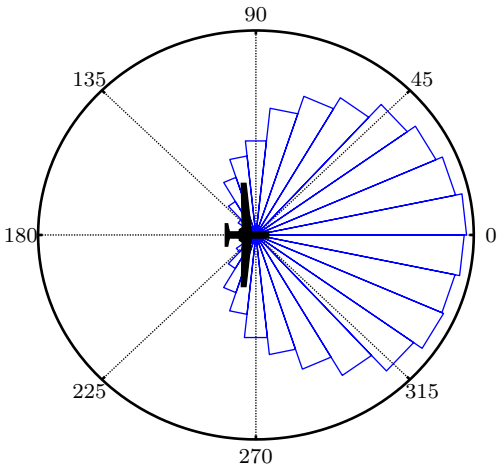

(b) Bearing distribution of 177,702 intruders initialized on the side of the encounter cylinder for Global Hawk/VFR encounters. The remaining 822,298 intruders for Global Hawk are initialized on the top or bottom of the cylinder due to the high climb and descent rates of Global Hawk

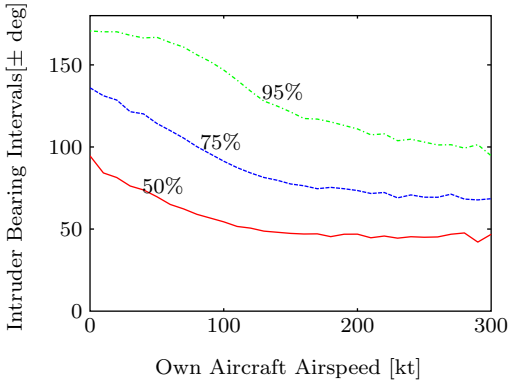

(c) Bearing intervals of intruder aircraft in VFR/VFR encounters as a function of the own aircraft's airspeed.

Figure 2. Initial intruder bearing characteristics.

IV. Electro-Optical Configuration Trade-offs

In the results that follow, we show tradeoffs between sensor field of view and detection performance, focusing only on those intruders that cause NMACs in our simulations. Data are plotted as the fraction of all NMAC intruders that were detected for the specified FOV and maximum sensor detection range along the ordinate against time until TMCD as the abscissa[a].

Figure 3 presents the fraction of NMAC-inducing intruders detected at each time step during the 40 second window prior to TMCD for VFR/VFR encounters with various sensor configurations. Figures 3(a) and 3(b) indicate that the sensitivity of these curves with respect to the FOV angles is locally small for the current design configuration. Slightly increasing or decreasing the azimuth and elevation angles has minimal impact on the fraction of NMAC intruders detected prior to TMCD. For example, increasing the azimuth angle of the FOV a total of 80° between ±90° and ±130° only results in approximately a 10% increase in the fraction of intruders detected at any point prior to TMCD.

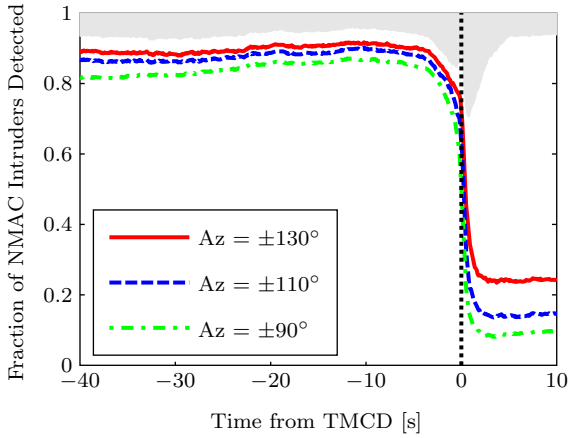

(a) Variable azimuth with a 5 NM detection range and ±15° elevation angle (TMCD=0).

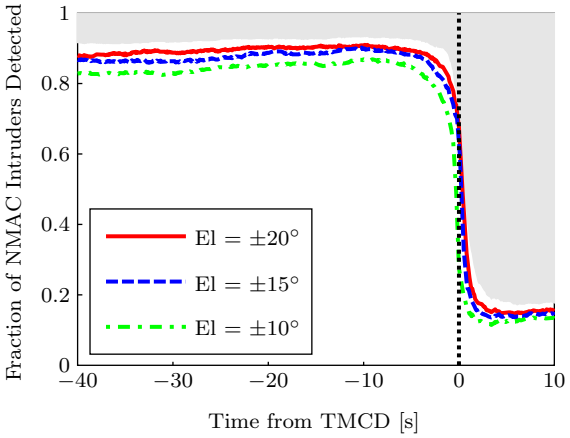

(b) Variable elevation with a 5 NM detection range and ±110° azimuth angle.

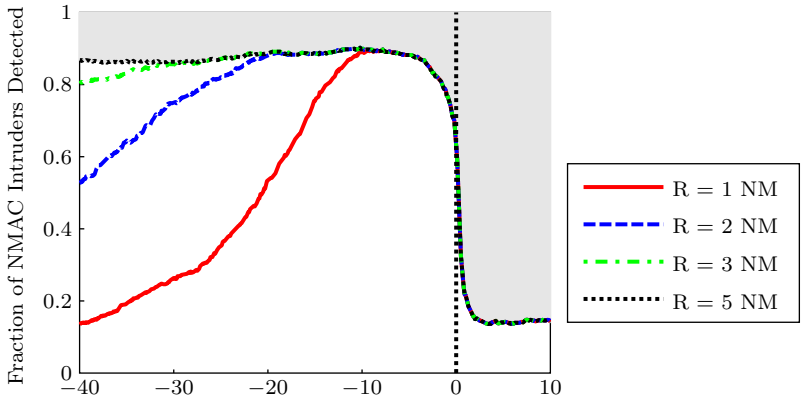

(c) Variable detection range with ±110° azimuth and ±15° elevation angles.

Figure 3. Fraction of NMAC-inducing intruders detected relative to TMCD for various sensor configurations in VFR/VFR encounters. The shaded gray regions correspond to infeasible detection values when varying the single configuration parameter. For example, a fraction of detected intruders equal to one cannot be achieved even if the FOV azimuth angle is increased to ±180° when the elevation angle is limited to ±15°.

Figure 3(c) covers a wide range of detection ranges because several uncontrollable factors such as intruder size, relative sun location, and atmospheric conditions may impact an EO sensor's detection range.[10] Increasing the detection range beyond 5 NM does not increase the fraction of intruders detected because the radius of our encounter cylinder is 5 NM. However, only one encounter in each encounter set caused an NMAC in under 40 seconds (less than 1% of NMACs). Thus, increasing the detection range beyond 5 NM is only necessary if the CAS requires more than 25 seconds to sense, track, and avoid an intruder aircraft. The current sensor is estimated to have a detection range of 3–4 NM, which is suitable for detecting most intrud-

ers with sufficient time for Global Hawk to avoid a collision (estimated to be 10–15 seconds).[5,11] Increasing the detection range of an EO sensor beyond 3–4 NM does not significantly increase the fraction of intruders detected within the 40 second window prior to TMCD. However, if the detection range is only 1 NM, then there is approximately only a 60% chance that the EO sensor detects an NMAC intruder at least 15 seconds prior to TMCD. This represents a significant reduction in sensor performance. If the degradation in EO detection range is known for certain conditions such as foggy weather, then one may estimate the reduced fraction of intruders detected when flying in those conditions.

The results from the Global Hawk/VFR encounters lead to slightly different conclusions (see figure 4). The fraction of detection curves with respect to detection range are nearly identical to the VFR/VFR encounters. However, the fraction of intruders detected is locally insensitive to changes in the FOV azimuth angle. The current, flight-tested sensor configuration with a ±100° azimuth angle is just as likely to detect an intruder prior to TMCD as an EO sensor that meets the standard configuration with a ±110° azimuth angle. In fact, the azimuth angle can be further reduced to ±90° without significantly degrading the fraction of intruders detected. Because Global Hawk's airspeed is higher than that of most intruders, there is a smaller probability that a VFR intruder will cause an NMAC from a large bearing angle (e.g., an overtaking encounter). Intruders in encounters that result in an NMAC with Global Hawk are more concentrated towards zero bearing in our simulation.

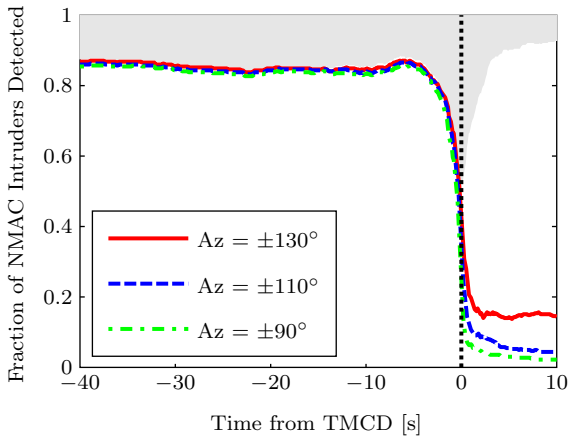

(a) Variable azimuth with a 5 NM detection range and ±15° elevation angle.

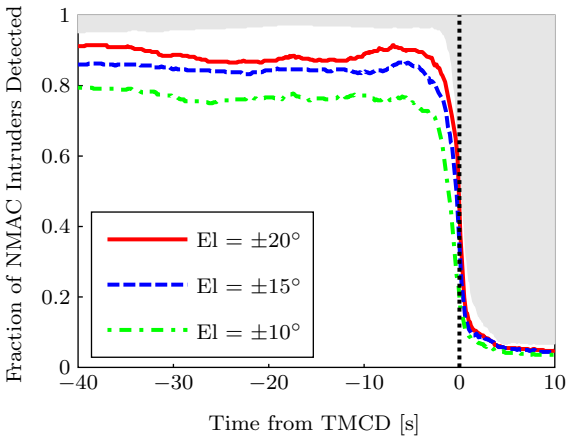

(b) Variable elevation with a 5 NM detection range and ±110° azimuth angle.

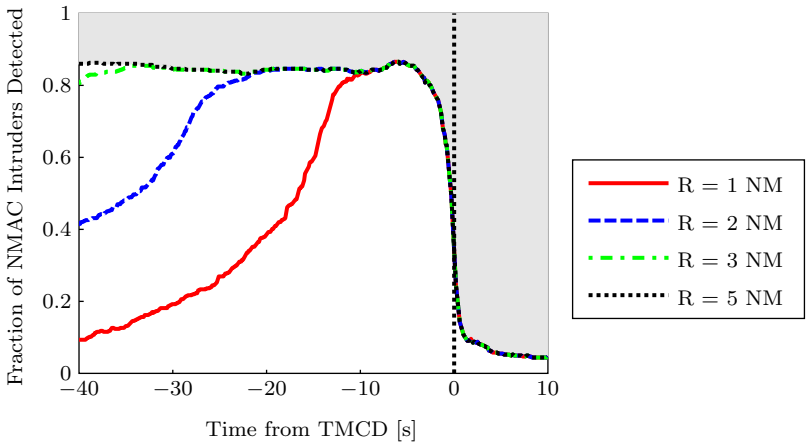

(c) Variable range with ±110° azimuth and ±15° elevation angles.

Figure 4. Fraction of NMAC-inducing intruders in view relative to TMCD with various sensor configurations for the Global Hawk/VFR encounters.

The FOV elevation angle on Global Hawk has a greater influence on the fraction of intruders detected than in the VFR/VFR encounter case. The increased sensitivity to elevation angle is a byproduct of the Global Hawk climb profile extracted from radar data. Due to the fact that Global Hawk is both climbing and turning, the FOV is not pointed in the direction of the future path of the vehicle. A significant portion

of NMAC intruders appear to be above the FOV, as shown in figure 5(a). One option to improve the fraction of intruders detected for the EO sensor is to increase the elevation angle over the entire FOV. However, there are other options. Reducing the frequency that Global Hawk turns as it climbs or descends through airspaces where encounters are likely to occur ensures that the FOV is pointed in the direction of the future path of the Global Hawk vehicle. Another option is to modify the EO sensor such that the FOV is bow-tie shaped where the middle, forward-facing camera has a small FOV with a high resolution while the outer cameras provide wide area coverage that capture intruders during turning maneuvers. One final option is to implement a horizontal stabilizer in the EO sensor. By counteracting the effect of the unmanned aircraft's bank angle nearly all of the intruders are in view within the 40 second window prior to TMCD as demonstrated in figure 5(b). On average, 23% more intruders are in the FOV per time-step when the EO sensor is horizontally stabilized for the Global Hawk climb profile from the radar data.

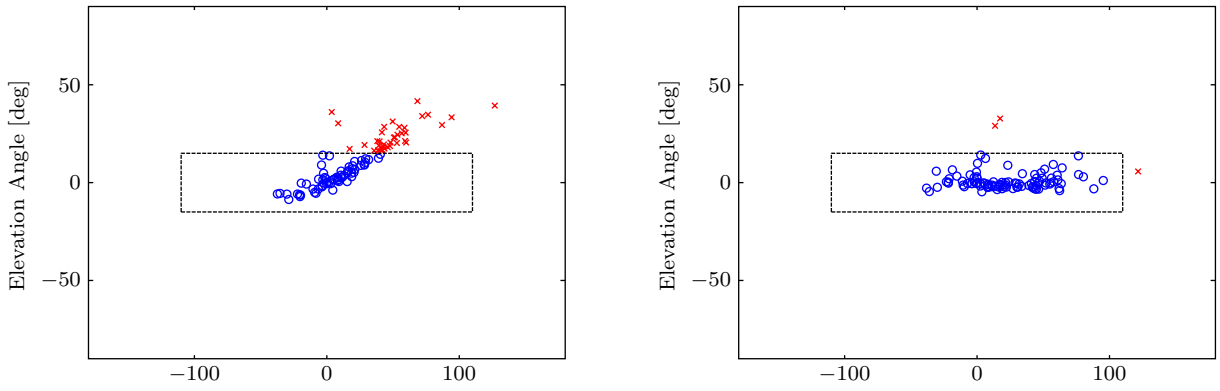

(a) Body-fixed FOV. (b) Horizontally-stabilized FOV.

Figure 5. Distribution of NMAC intruders in the EO sensor FOV 15 seconds prior to TMCD for the Global Hawk climb profile observed from radar data. Blue circles indicate that the intruder is in the FOV while red crosses indicate that the intruder is outside the FOV.

Previous studies claim that a slightly reduced FOV ($\pm 100^\circ$ azimuth angle) is desirable for testing purposes since it is significantly less expensive to develop—using a commercial off-the-shelf EO system reduces the price of the system by a factor of ten.[5] Our analysis suggests that upgrading the FOV azimuth angle to $\pm 110^\circ$ does not appreciably increase system performance due to the airspeed of Global Hawk in our simulation. Instead, better performance may be realized by improving detection range or increasing the elevation angle. While the current estimated detection range is suitable for nominal conditions, several factors such as weather and intruder aircraft size may reduce the effective detection range of the EO sensor.

V. Effect of Azimuth Angle on Fraction of Intruders Detected

The previous section addressed the advantages and disadvantages of improving or degrading individual EO sensor configuration parameters. In general, however, a measurable trade-off exists between different parameters. For example, increasing the solid angle subtended by the FOV decreases the detection range of an EO sensor with a fixed pixel array and detection technology because the sensor's resolution is degraded. Concentrating the FOV over a small area improves the detection of head-on encounters where closure rates are generally higher but reduces detection of slow-closing intruders from the side of the aircraft. Figure 6 is a conceptual example of this tradeoff between azimuth angle and detection range.

In this study we evaluate the effect that varying the FOV azimuth angle has on the fraction of NMAC intruders detected prior to TMCD for a fixed sensor resolution. As before, an intruder is in view if both the relative azimuth and elevation angle of the intruder aircraft are within the FOV of the EO sensor. However, we now consider the projected area of the intruder aircraft on the pixel sensor array. If the projected area is greater than the sensor resolution of the pixel array grid, then the intruder is detected.

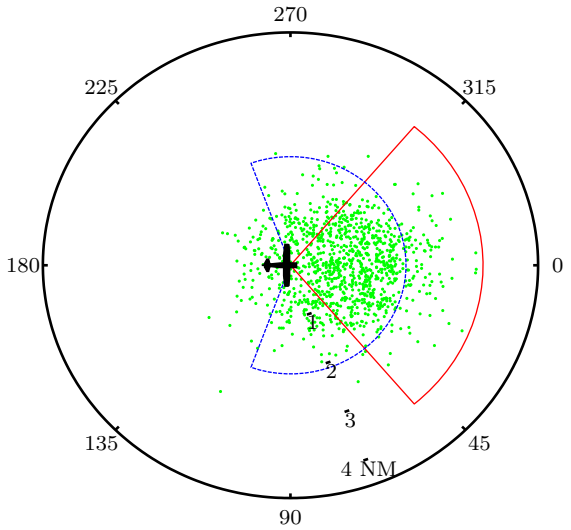

Figure 6. Plan view of all 541 NMAC intruders from the VFR/VFR encounter set 20 seconds prior to TMCD. The two FOVs are notional examples of the tradeoff between azimuth angle and detection range.

V.A. Approach

We define the detection threshold Ω as the minimum proportion of the angle subtended by the EO sensor's FOV required for the tracking algorithm to detect the intruder aircraft. Consider an EO sensor with three cameras, each with a pixel array grid that is 2000 by 1000. If the minimum intruder detection threshold requires that the intruder is projected on at least one pixel, then $\Omega = 1/(3{\cdot}2000{\cdot}1000) = 1.67{\cdot}10^{-7}$. Thus, if the projected area of the intruder aircraft is at least $1.67{\cdot}10^{-7}$ of the entire angle subtended by the FOV, then the intruder is detected. Analyzing fraction of intruders detected based on Ω reduces a two-dimensional problem in terms of the number of pixels in the EO sensor array and sensor resolution (i.e. minimum number of pixels onto which the aircraft is projected that is required for detection) into a single-dimensional problem. Although Ω is a dimensionless variable, we write Ω with the units μsr/sr for clarity.

We calculate the projected visual area of an aircraft using a three-dimensional polygon model of the aircraft. First, we project the model onto the visual plane of the own aircraft. Then we calculate the union of the projected polygons to determine the projected area. The solid angle subtended by the aircraft is then calculated by dividing the projected visual area by the square of the range to the intruder aircraft. Because the encounter model does not specify an aircraft body type, we consider two different aircraft for this study whose properties are summarized in table 3. These aircraft represent extremes in size of intruder that may be expected for VFR aircraft.

Table 3. Aircraft properties.

	Length (ft)	Wingspan (ft)	Wing Area (ft^2)
Narrow body (Boeing 737)	110.3	117.4	1,345.4
Ultralight (CGS Hawk Ultra)	20.7	28.9	135.0

V.B. Results

Figure 7 presents the fraction of intruders detected 30 and 10 seconds prior to TMCD for VFR/VFR encounters. In these figures, $\Omega = 1/6\,\mu$sr/sr corresponds to a one pixel detection threshold for the current pixel array configuration, while $\Omega = 2/3\,\mu$sr/sr corresponds to a four pixel detection threshold. The results in these figures demonstrate that the current sensor detection technology is sufficient for detecting narrow-body (and larger) aircraft prior to TMCD with sufficient time to initiate an avoidance maneuver. In addition, increasing sensor resolution increases the fraction of Boeing 737 intruders that are detected. If all intruders are anticipated to be Boeing 737s, then it is sensible to make the FOV azimuth angle as large as possible.

Results with ultralight intruders are noticeably different. Thirty seconds prior to TMCD, the current sensor's fraction of ultralight intruders detected is 0.63 and 0.24 when $\Omega = 1/6\,\mu$sr/sr and $2/3\,\mu$sr/sr, respec-

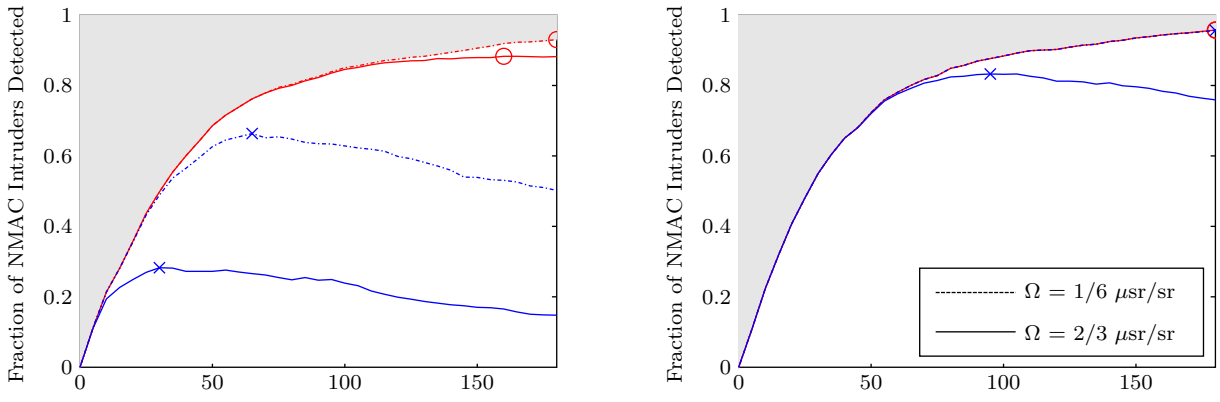

(a) 30 seconds prior to TMCD.

(b) 10 seconds prior to TMCD.

Figure 7. Trade-off curves between FOV azimuth angle and fraction of intruders detected for fixed Ω values. The red curves in these figures correspond to Boeing 737 intruders and the blue to ultralight intruders where an "o" and an "x" denote the optimal azimuth angle operating point for each aircraft, respectively. The gray areas shade out infeasible areas due to FOV limits even if there is no minimum projected visual area required for detection.

tively. In addition, increasing the current configuration FOV azimuth angle actually reduces the fraction of small intruder aircraft detected. Instead, improved performance is realized by decreasing the azimuth angle. Assuming an aircraft requires approximately 10 to 20 seconds to detect, track and avoid an intruder aircraft, then the azimuth angle that provides the highest fraction of detection for ultralight intruders in VFR/VFR encounters is between ±50° and ±100° in our simulations.

Reducing the current FOV azimuth angle for Global Hawk is certainly feasible. Trade-off curves from Global Hawk/VFR encounters (not shown) demonstrate that the FOV azimuth can be reduced to approximately ±90° without any reduction in the fraction of narrow-body intruders detected. At the same time, the fraction of ultralight intruders detected is increased because the projected area required for detection is lower with a smaller FOV azimuth angle. Decreasing the FOV azimuth angle from ±100° to ±90° increases the fraction of ultralight intruders detected between 0.02 and 0.05 depending on the value of Ω.

Several previous studies hypothesize that general aviation represents the largest risk of collision for unmanned aircraft because general aviation aircraft are generally lower-flying, flown by inexperienced pilots, and may be flying without the aid of air traffic control.[11,12] Because general aviation aircraft are typically smaller than commercial aircraft, reducing the current EO sensor FOV may improve Global Hawk's sense and avoid capability. These results also suggest that the current EO sensor FOV configuration, while smaller than the current FOV standard with an azimuth angle of ±110°, provides slightly better performance than if the sensor met the current FOV requirements in our simulations.

VI. Conclusions and Future Work

This paper addressed the design of an EO system to provide a sense and avoid capability on Global Hawk and other unmanned aircraft. We analyzed the effect that changing the FOV azimuth and elevation angles, in addition to detection range, has on the fraction of intruder aircraft detected prior to TMCD. We also assessed the trade-off between FOV azimuth and fraction of various sized intruders being detected prior to an NMAC occurring. The fidelity of our study is a result of the encounter model, which provides a statistical representation of VFR traffic and likely encounters in U.S. airspace. Note that we did not study encounters with IFR aircraft where the closing speeds and encounter geometry are likely very different than in this model.

Our analysis suggests that the current EO system being flight-tested on Global Hawk is suitable for detecting larger aircraft but may not be ideal for detecting smaller aircraft with enough lead time for Global Hawk to avoid an NMAC in our simulation. In addition, we observed that the FOV azimuth angle for Global Hawk can be reduced to ±90° with little degradation in the fraction of VFR intruder aircraft detected prior to near miss. Since Global Hawk flies faster than most of the aircraft in our VFR encounter model, the distribution of intruders is more concentrated towards zero bearing than most VFR traffic. This observation

suggests that the FOV which maximizes the fraction of intruders detected for an EO system—and, therefore, the level of safety while flying the unmanned aircraft—is a function of both the unmanned aircraft's airspeed and flight profile. A slow flying unmanned aircraft requires a wider FOV than a faster aircraft since overtaking encounters are more likely to occur. In contrast, the faster vehicle requires a larger detection range because the closure rates of intruder aircraft are generally higher.

This work presents a foundation for future studies and analyses of CAS for unmanned aircraft. First, the analysis in this paper included a limited set of Global Hawk profiles. A more thorough analysis of Global Hawk sense-and-avoid capabilities requires higher fidelity models of anticipated flight profiles. A logical extension for the Global Hawk EO system is to analyze a nonuniform EO sensor FOV. A system where the center camera has a smaller FOV but larger detection range may lead to improved detection performance. Finally, future research requires sensor models that incorporate the challenges of accurately detecting intruder aircraft due to false tracks and missed detections. Previous flight tests have shown that false tracks are still a major obstacle for EO systems.[6] Incorporating accurate sensor models are likely to affect the conclusions presented in this paper.

Acknowledgements

This work is sponsored by the Air Force under Air Force Contract #FA8721-05-C-0002. Opinions, interpretations, conclusions, and recommendations are those of the authors and are not necessarily endorsed by the United States Government. This report is the result of research and development sponsored by the the United States Air Force 303rd Aeronautical Systems Wing (303 AESW/XRX), and the Department of Defense Unmanned Aircraft System Airspace Integration Joint Integrated Product Team.

References

[1]Kochenderfer, M. J., Espindle, L. P., Kuchar, J. K., and Griffith, J. D., "A Bayesian Approach to Aircraft Encounter Modeling," *Proceedings of the AIAA Guidance, Navigation and Control Conference*, 2008.

[2]Ebdon, M. D. and Regan, J., "Sense-and-Avoid Requirement for Remotely Operated Aircraft (ROA)," White Paper OPR: HQ ACC/DR-UAV SMO, Air Combat Command, June 2004.

[3]Federal Aviation Administration, "Order 7610.4K: Special Military Operations," February 2004.

[4]ICAO, "Rules of the Air," *Annex 2 to the Convention on International Civil Aviation*, No. 9, 1990.

[5]McCalmont, J., Utt, J., Deschenes, M., and Taylor, M., "Sense and Avoid, Phase I (Man-in-the-Loop) Advanced Technology Demonstration," *Infotech@Aerospace*, 2005, Arlington, VA, September 2005.

[6]Utt, J., McCalmont, J., and Deschenes, M., "Development of a Sense and Avoid System," *Infotech@Aerospace*, American Institute of Aeronautics and Astronautics, Arlington, VA, September 2005.

[7]Carnie, R., Walker, R., and Corke, P., "Image Processing Algorithms for UAVs "Sense and Avoid"," *IEEE International Conference on Robotics and Automation*, 2006.

[8]Grappel, R. D., "ASR-9 Processor Augmentation Card (9-PAC) Phase II Scan-Scan Correlator Algorithms," Tech. Rep. MIT-LIN-ATC-298, MIT Lincoln Laboratory, April 2001.

[9]Gertz, J. L., "Mode S Surveillance Netting," Tech. Rep. MIT-LIN-ATC-120, MIT Lincoln Laboratory, Nov. 1983.

[10]Chen, W.-Z., Portilla, E., Clough, B., and Molnar, T. J., "See and Avoid Sensor System Design Part II—System Reliability & Cost/Benefits," American Institute of Aeronautics and Astronautics, San Diego, CA, September 2003.

[11]Schaefer, R. J., "A Standards-Based Approach to Sense-and-Avoid Technology," *Unmanned Unlimited Technical Conference, Workshop and Exhibit*, American Institute of Aeronautics and Astronautics, Chicago, Il, September 2004.

[12]Chen, W.-Z. and Molnar, T. J., "Autonomous Flight Control Sensing Technology (AFCST) Program Phase I —Capability Goals and Sensing Requirements," Technical Paper AFRL-VA-WP-TP-2002-309, Air Force Research Laboratory, Wright-Patterson Air Force Base, OH, July 2002.